PHYSICAL REVIEW C

NUCLEAR PHYSICS

THIRD SERIES, VOLUME 57, NUMBER 1 JANUARY 1998

RAPID COMMUNICATIONS

The Rapid Communications section is intended for the accelerated publication of important new results. Manuscripts submitted to this section are given priority in handling in the editorial office and in production. A Rapid Communication in **Physical Review C** *may be no longer than five printed pages and must be accompanied by an abstract. Page proofs are sent to authors.*

Triaxial superdeformed bands in ^{86}Zr

D. G. Sarantites,[1] D. R. LaFosse,[1,*] M. Devlin,[1] F. Lerma,[1] V. Q. Wood,[2] J. X. Saladin,[2] D. F. Winchell,[2] C. Baktash,[3] C.-H. Yu,[3] P. Fallon,[4] I. Y. Lee,[4] A. O. Macchiavelli,[4] R. W. MacLeod,[4] A. V. Afanasjev,[5,†] and I. Ragnarsson[5]

[1]*Chemistry Department, Washington University, St. Louis, Missouri 63130*

[2]*Physics Department, University of Pittsburgh, Pittsburgh, Pennsylvania 15260*

[3]*Physics Division, Oak Ridge National Laboratory, Oak Ridge, Tennessee 37831*

[4]*Nuclear Science Division, Lawrence Berkeley National Laboratory, Berkeley, California 94720*

[5]*Department of Mathematical Physics, Lund Institute of Technology, Box 118, S-22100 Lund, Sweden*

(Received 22 August 1997)

Four new superdeformed bands have been found in the nucleus ^{86}Zr. The good agreement between experiment and configuration-dependent shell correction calculations suggests that three of the bands have triaxial superdeformed shapes. Such unique features in mass $A\sim80$ superdeformed bands have been predicted, but not observed experimentally until now. A fourth band in ^{86}Zr is interesting due to a fairly constant and unusually high dynamic moment of inertia. Possible interpretations of this structure are discussed. [S0556-2813(98)50101-X]

PACS number(s): 21.10.Re, 21.60.Cs, 23.20.Lv, 27.50.+e

The study of superdeformed (SD) nuclei has been at the forefront of nuclear structure research during the last decade. With the advent of large γ-ray detector arrays, new regions of SD nuclei have been uncovered encompassing mass $A\sim80$ [1] and $A\sim60$ [2]. Detailed studies of SD in these mass regions have been mainly due to the coupling of Gammasphere [3] with the Microball [4], a 4π charged-particle detector array.

SD structures in the $A\sim80$ region possess many surprising features. In ^{87}Nb two bands were found to mutually interact; one of these bands undergoes a second interaction interpreted through the influence of the $N=6$ $i_{13/2}$ ''superintruder'' orbital [5]. Bands have also been observed to branch out into different decay paths [6,7]. The sensitivity of the shapes of these structures to changes in neutron number has also been demonstrated in the $_{38}$Sr isotopes [8]. In this report, detailed calculations using the configuration-dependent shell correction method [9,10] have been performed for direct comparison to known SD states in ^{86}Zr. The calculations suggest that these structures possess significantly nonaxial shapes, having $\gamma\sim20°$. Earlier calculations in the mass $A\sim80$–90 region suggest a variety of shapes at high spin in these nuclei [10,11]. This and a prior report on SD in ^{80}Sr [8] are the first experimental indications of these exotic nuclear shapes. Previously, evidence for the existence of triaxial SD shapes has only been found experimentally in ^{163,165}Lu [12].

The experiment was performed at the 88-Inch Cyclotron at E. O. Lawrence Berkeley National Laboratory. A self-supporting 380 μg/cm^2 foil of highly enriched ^{58}Ni was bombarded by a 134-MeV ^{31}P beam with intensity 2–4 $\times10^{10}$ s^{-1}. Gamma rays were detected by the Gammasphere array with 86 Ge detectors and 10 additional BGO anti-Compton shields in place without Ge detectors. The Hevimet collimators for all BGO shields were removed providing γ-ray fold (k_γ) and sum energy (H_γ) for each event [13]. Light charged particles (p,d,t,α) were detected with the Microball. The event trigger was determined by three- or higher-fold Ge-coincidences, accepting any related coincidences with the Microball. A total of 3×10^9 events were acquired in 3.5 days.

*Current address: Department of Physics, State University of New York at Stony Brook, Stony Brook, NY 11794.

†Permanent address: Nuclear Research Center, Latvian Academy of Sciences, Salaspils, Latvia, LV-2169.

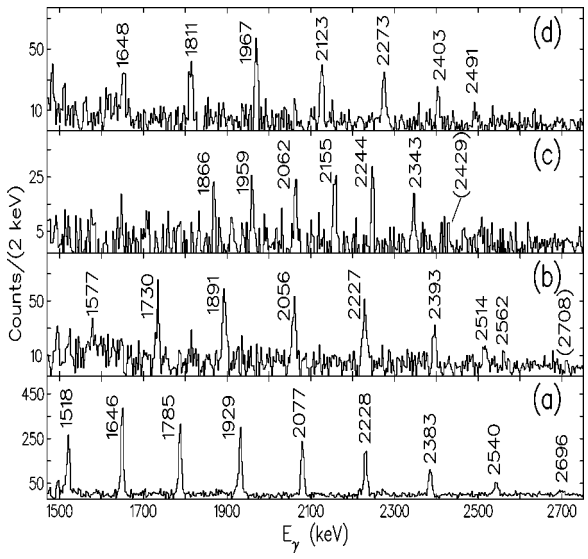

FIG. 1. Spectra showing all four SD bands, obtained by double gating on all transitions, requiring 2 or 3 protons and $k_\gamma \geqslant 17$. Panels (a), (b), (c), and (d) show the spectra for SD1, SD2, SD3, and SD4, respectively.

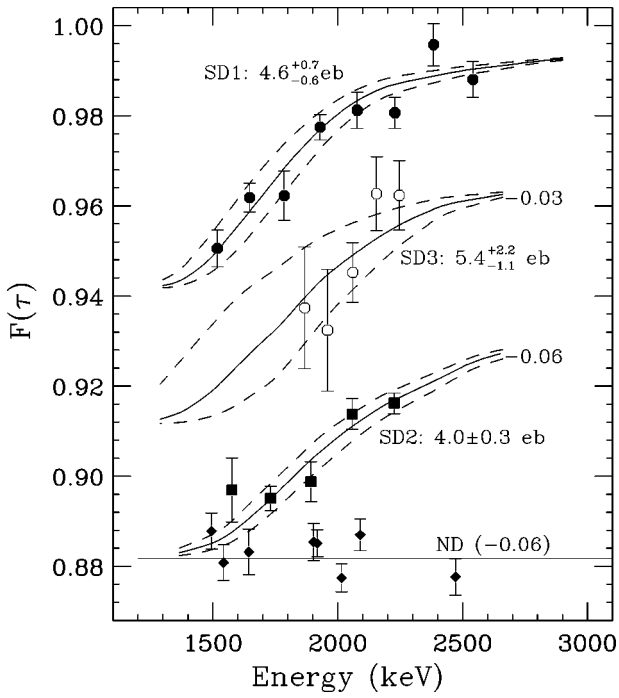

FIG. 2. Fractional Doppler shift as a function of transition energy for SD bands in ^{86}Zr. Filled circles represent SD1, filled squares SD2 (shifted by -0.06), open circles SD3 (shifted by -0.03) and filled diamonds represent escaping normally deformed (ND) recoils (shifted by -0.06). The solid curves are calculations with the indicated Q_t values; the dashed curves correspond to one standard deviation as indicated.

The charged particles were identified by two coupled pulse-shape discrimination techniques [4]; a single proton detection efficiency of 84% was attained. The events were sorted according to charged particle gates, i.e., $2p$, $3p$, αp, etc. The $3p$-gated events leading to ^{86}Zr were 18% of the total, and contained small amounts of the $\alpha 3p$ and $4p$ channels due to particles escaping detection. The statistics were increased by a factor of ~ 1.7 by including $2p$ gated events, giving a total of 5.4×10^8 events. Of these 78% were ^{86}Zr ($3p$) and ^{85}Zr ($3pn$) in the ratio of 1:6, the remainder consisting of the $2pn$, $\alpha 2p$, $4p$, and $\alpha 3p$ channels. In order to enhance the high-spin content of the data, a γ-ray fold requirement of $k_\gamma \geqslant 17$ was applied. This removed 90% of the ^{85}Zr with a modest loss of 35% and 25% of the total ^{86}Zr and SD counts, respectively. The data were sorted into E_γ-E_γ coincidence matrices and E_γ-E_γ-E_γ cubes for analysis with the Radware [14] software package.

Examination of the matrices and cubes revealed four sequences of mutually coincident γ rays shown in Fig. 1. The four bands have been assigned to ^{86}Zr through charged particle gates, and coincidences with only low-spin transitions in ^{86}Zr. Relative to the total intensity of ^{86}Zr, bands SD1 through SD4 were populated to $2.0\pm 0.2\%$, $0.6\pm 0.1\%$, $0.5\pm 0.1\%$, and $0.24\pm 0.08\%$, in order, requiring $k_\gamma \geqslant 17$. The $E2$ nature of all, but the weakest transitions in the bands was established from directional correlation (DCO) ratios [15] of transitions observed near 90° and 0° relative to the beam. The spins of the states in SD1 were estimated through the decay of SD1 into normally deformed (ND) states of known spin. This analysis yields $I_0 = 21.7\pm 1.5\hbar$ for the spin of the bottom state of SD1. It was not possible to assign reliable spins to the weaker bands in this manner. However, all the SD bands were found to have nearly the same average k_γ values suggesting spins similar to SD1. Note also that at low spins the transition energies of SD4 are at the midpoint of those of SD2. Thus it is assumed that the two bands are signature partners and the spins of SD4 $1\hbar$ higher than those of SD2.

Since the SD bands are expected to decay, while the recoiling nuclei are traversing the target, it is possible to estimate the lifetimes, and hence the transition quadrupole moments (Q_t) of the bands using the residual Doppler-shift attenuation method [16]. To this end, six asymmetric matrices were sorted with all detectors incremented on one axis and those having six values of $(\cos\theta)_{\rm avg}$ between 0.8226 and -0.8667 on the other axis. As before these were gated by $3p$ or $2p$ and $k_\gamma \geqslant 17$. The centroids of the SD lines were determined as a function of $(\cos\theta)_{\rm avg}$ for each band by gating on all possible transitions in the band. Least squares fits provided the fractional Doppler shift, $F(\tau)$, for each transition. Some of the results are shown in Fig. 2 together with the Q_t values extracted using the model described in Refs. [16,17]. The measured Q_t for SD1 through SD4 are, in order, $4.6^{+0.7}_{-0.6}$, 4.0 ± 0.3, $5.4^{+2.2}_{-1.1}$, and $3.8^{+0.6}_{-0.5}$ eb. One should note that the uncertainties reported are only statistical, and do not include any estimate of systematic errors. The Q_t values for these structures are consistent with those measured for other $A\sim 80$ SD bands.

In order to gain a theoretical understanding of these SD bands, configuration-dependent shell correction calculations employing a cranked Nilsson potential have been performed using the approach of Ref. [9]. In the present approach [10], we have the ability to identify the high-j orbitals in each N-shell after the diagonalization. This technique allows us to distinguish between the particles of (approximate) $g_{9/2}$ character and the particles belonging to other $N=4$ subshells ($g_{7/2}, d_{5/2}, \ldots$). The calculations are carried out in a mesh in the deformation space, $(\varepsilon_2, \varepsilon_4, \gamma)$. Then for each fixed con-

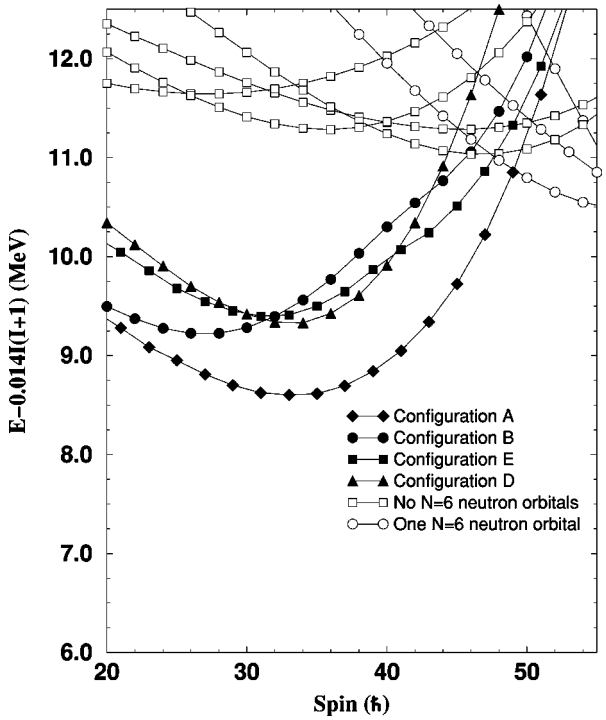

FIG. 3. Theoretical calculations of the energies of superdeformed states (minus a rigid rotor reference) versus spin. Filled symbols denote triaxial SD configurations with a $\pi 5^1 \nu 5^2$ structure, open symbols those having larger deformation near-prolate SD shapes. Note there is no configuration labeled C; see text for details.

figuration and each spin separately, the total energy is determined by a minimization in the shape degrees of freedom. Pairing correlations are neglected in the calculations because they are of small importance in the spin range of interest [11]. The transition quadrupole moment Q_t is calculated from equilibrium deformations $\varepsilon_2, \varepsilon_4, \gamma$ using Eqs. (3)–(5) of [18]. Standard parameters of the Nilsson potential [9] have been used in calculations.

Partial results including only SD states are shown in Fig. 3 where a rigid rotor reference has been subtracted from the energies. Two groups of highly deformed states can be seen. Those lowest in energy over the spin range $I=20$–$45\hbar$ all have triaxial SD shapes. These configurations have one proton and two neutron $N=5$ ($h_{11/2}$) orbitals occupied ($\pi 5^1 \nu 5^2$). Some of these configurations have been given labels A, B, D, and E in the figure. (A configuration designated C which will be used in our interpretation was not included due to difficulties in the calculation, see below.) The triaxiality of these configurations is illustrated in Fig. 4, which shows potential energy surfaces of configuration A. Note that the lowest minimum at spin $I=39$ corresponds to a nuclear shape having a high degree of triaxiality, $\gamma \sim 20°$, approximately 1 MeV below the lowest energy for axial shape, $\gamma = 0°$. The second group of states lies very high in energy and becomes yrast at $I \sim 48\hbar$. These states have an enhanced prolate deformation, $\varepsilon_2 \geq 0.6$, and involve additional $N=5$ orbitals and in some cases also the $N=6$ neutron superintruder orbital. One should note that several configurations involving fewer $N=5$ orbitals, and also $\pi 5^2 \nu 5^2$ configurations are not shown in Fig. 3 for clarity. These configurations are ruled out as candidates for the observed SD bands

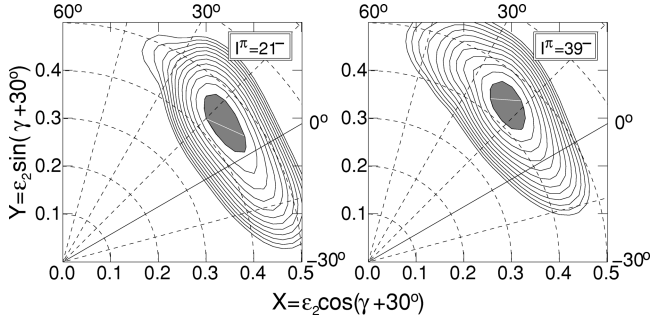

FIG. 4. Potential energies surfaces for spins $I=21\hbar$ and $I=39\hbar$ for configuration A. The radial coordinate of these plots is the quadrupole deformation parameter ε_2, and the angular coordinate is the triaxiality parameter γ. Contour lines separate energies differing by 0.25 MeV and the last contour line corresponds to 3.0 MeV excitation with respect to the shaded minimum.

due to either low collectivity or high excitation energies in the spin range of interest. The calculated single particle energies for protons and neutrons, employing a Nilsson potential with the standard parametrization [9] and $\varepsilon_2=0.44$, $\varepsilon_4=0.035$, and $\gamma=20°$ are shown in Fig. 5. The deformation parameters are typical of those calculated at spin $I \sim 40\hbar$ for the lowest energy configurations of Fig. 3. The deformation

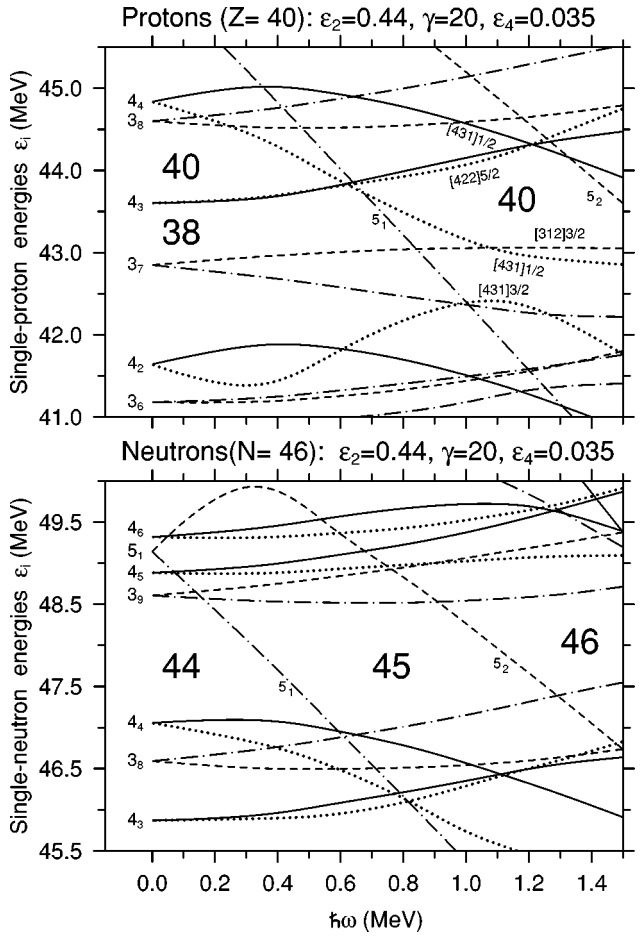

FIG. 5. Calculated proton and neutron Nilsson single particle energies. Linetypes denote the parity and signature of the orbitals (π,α) as follows: solid $(+,+1/2)$, dotted $(+,-1/2)$, dashed $(-,+1/2)$, and dash-dotted $(-,-1/2)$.

TABLE I. Calculated deformation parameters for the configurations A, B, D, and E.

Configuration	Spin ($\hbar$)	ε_2	γ (deg)
A	21	0.450	11.9
	39	0.443	19.0
B	20	0.443	12.8
	40	0.428	18.9
D	20	0.477	17.8
	40	0.470	27.1
E	21	0.476	20.1
	39	0.475	25.6

parameters for the configurations A, B, D, and E can be found in Table I.

Direct comparisons between the experimental data and calculations are shown in Fig. 6. In Fig. 6(a) the dynamic moments of inertia ($\mathcal{J}^{(2)}$) of the four SD bands are shown, along with the calculated $\mathcal{J}^{(2)}$ for configurations A and B; part (b) shows theoretical and experimental effective alignments ($i_{\rm eff}$). The following spins for the lowest observed states in the SD bands were used: SD1: $I_0=23\hbar$; SD2: $I_0=22\hbar$; SD3: $I_0=25\hbar$; SD4: $I_0=23\hbar$. These are consistent with the estimated spins, but reflect the configurations assigned to the bands below.

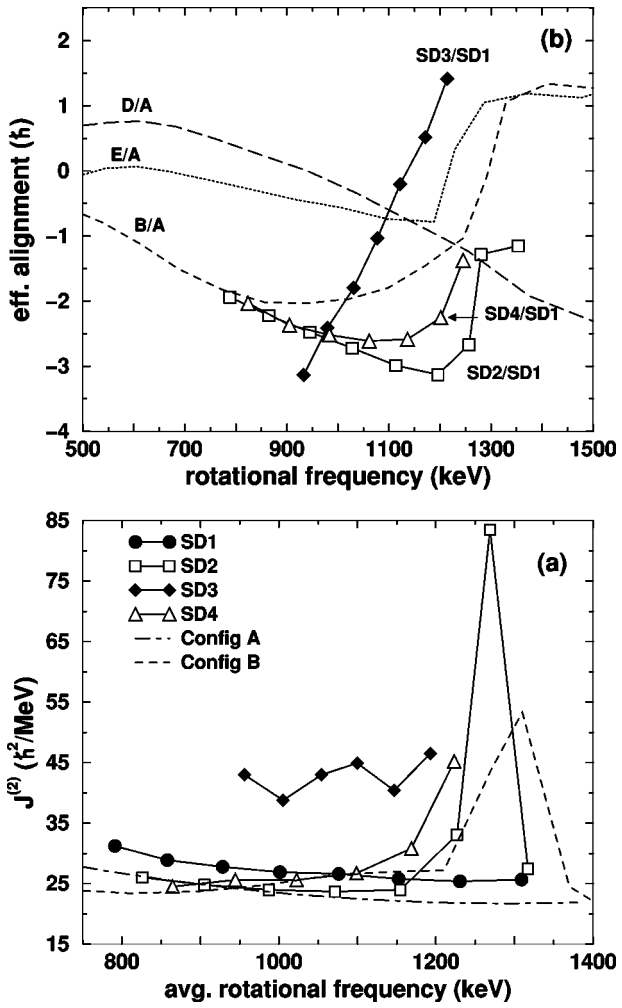

FIG. 6. (a) Experimental dynamic moments of inertia for the four SD bands in ^{86}Zr. Also shown are the calculated dynamic moments of inertia for configurations A and B. (b) Experimental effective alignments (in units of $\hbar$) of SD2 through SD4 relative to SD1. Theoretical effective alignments for configurations B, D, and E relative to configuration A are shown as well. In our preferred scenario SD2 is associated with configuration B and SD 4 with C (not shown), see text for details.

The lowest-energy configuration A (Fig. 3) can be associated with SD1. In this configuration, all single-particle orbitals below the $Z=40$ and $N=46$ SD shell gaps at $\hbar\omega\geqslant 1$ MeV in Fig. 5 are occupied. One could note that these gaps are closely related to the axis ratio 2:1 shell gaps present at particle number 44 seen in, for example, Fig. 2 of Ref. [9]. Relative to this gap, two neutrons are added in the upsloping 3_8 orbital in Fig. 5 to achieve the $N=46$ configuration, while two protons are removed from the [422]5/2 orbitals and one from each of the [431]1/2 and 5_2 to get the $Z=40$ configuration. This configuration has parity $\pi=-$ and signature $\alpha=1$. The population of this band is ~ 4 times higher than the other three bands, suggesting SD1 is significantly lower in energy at comparable spins, as is configuration A. The calculated $\mathcal{J}^{(2)}$ of this band also agrees with the experimental data, see Fig. 6. Not only is the magnitude of the $\mathcal{J}^{(2)}$ reproduced, but also the downward slope. This trend is related to an increase in the triaxiality of the nuclear shape with increasing spin, see Fig. 4. The experimental Q_t value of $4.6^{+0.7}_{-0.6}$ eb for SD1 agrees well with calculated mean value of 4.2 eb averaged over the estimated spin range of SD1.

As mentioned previously, SD2 and SD4 are likely signature partners with small signature splitting. Interpretation of these two bands is therefore based on the signature partner [422]5/2 orbitals, which can be seen in Fig. 5 to have small signature splitting over the rotational frequency range of interest. Two signature partner bands can be created by exciting a proton from the [312]3/2 $\alpha=1/2$ or the [431]1/2 $\alpha=-1/2$ orbitals to either of the [422]5/2 orbitals.

Configurations B and C are the result of proton excitations from the [431]1/2 $\alpha=-1/2$ orbital to the positive and negative signature [422]5/2 orbitals, respectively. Assigning SD2 to configuration B and SD4 to C best fit the experimental data. One should note that since the orbitals belonging to low-j $g_{7/2},d_{5/2}\ldots$ subshells are treated in our calculations as one entity, it was not possible to trace the configuration C. However, since configurations B and C are signature partners based on [422]5/2 orbitals with small signature splitting, it is reasonable to expect that calculated properties of these configurations are similar in the rotational frequency range of interest. One important difference between them is that at a rotational frequency of $\hbar\omega\sim 1.3$ MeV, the [422]5/2 $\alpha=1/2$ orbital is crossed by the [431]1/2 $\alpha=1/2$ orbital, resulting in the sharp increase in the calculated $\mathcal{J}^{(2)}$ of configuration B. This is in agreement with the experimental $\mathcal{J}^{(2)}$ for band SD2 which shows a similar peak. This crossing will not be present in configuration C, since the [422]5/2 $\alpha=1/2$ orbital is unoccupied. A small increase in the $\mathcal{J}^{(2)}$ at the highest frequencies is expected, however, due to the crossing with strong interaction of the [431]1/2 and [431]3/2 $\alpha=-1/2$ orbitals. This is in agreement with the experimental $\mathcal{J}^{(2)}$ of SD4. Note that this crossing will also be present in SD2, but

that it is obscured by the prominent [422]5/2-[431]1/2 crossing. Finally, the measured Q_t is in agreement with the theoretical estimates. SD2 has $Q_t = 4.0 \pm 0.3$ eb; that calculated for configuration B, averaged over the observed spin range of SD2, is 4.0 eb. In addition, the measured value $Q_t = 3.8^{+0.6}_{-0.5}$ for SD4 is close to the one of SD2 which is reasonable considering the signature partner interpretation of these bands.

The calculated effective alignments for the pair of configurations B/A is in good agreement with experiment for the pair SD2/SD1 at low rotational frequencies, while with increasing rotational frequency the discrepancy grows. In our interpretation, this is connected to the interaction between the [431]1/2 and [431]3/2 $\alpha = -1/2$ orbitals (see Fig. 5). If the crossing between these orbitals were shifted to higher rotational frequencies, the discrepancy between calculations and experiment would become smaller. Considering that the employed parameterization of the Nilsson potential may not be optimal, this can be achieved by fitting the relative energies of the $\pi g_{9/2}$ and $\pi g_{7/2}$ subshells.

The above assignments best agree with the experimental results, however a second possibility deserves brief mention. Configurations D and E result from the excitation of a proton from the [312]3/2 $\alpha = 1/2$ orbital to the negative and positive signature [422]5/2 orbitals, respectively. These configurations have average calculated quadrupole moments of ~ 4.0 eb, in agreement with experiment. However, this configuration assignment appears less likely because a consistent interpretation does not emerge. In particular, the effective alignment of configuration D relative to configuration A is smoothly decreasing and does not resemble the experimental alignments of either the SD2/SD1 or SD4/SD1 pairs.

Finally, the experimental effective alignment of the SD4/SD1 pair comes reasonably close to the calculated alignment in the E/A pair if the spin $I_0 = 25\hbar$ is used for lowest observed state in band SD4. This may suggest that bands SD2 and SD4 are in fact not signature partners, but that SD2 can be associated with configuration B and SD4 with configuration E. Note however, that this interpretation does not explain the observed signature degeneracy of SD2 and SD4 at low spins, which suggests that the two bands are built on the same orbital.

The interpretation of SD3 is rather uncertain. This band is intriguing due to the high $\mathcal{J}^{(2)}$ and drastically increasing $i_{\rm eff}$. The high value of the $\mathcal{J}^{(2)}$ can be due either to enhanced deformation, or multiple crossings which occur over a fairly short range of rotational frequency. However, the calculations for both the triaxial superdeformed bands and the enhanced deformation bands do not agree with the experimental data for SD3. In addition, the association of SD3 with one of the enhanced deformation configurations would be rather tenuous. These configurations are very high in energy, and are only yrast at high spins that are not likely to be populated in the experiment. The $\mathcal{J}^{(2)}$ of SD3 is actually higher than that of the calculated enhanced deformation configurations; hence the slope of the $i_{\rm eff}$ is underpredicted as well. Besides, the irregularity of the $\mathcal{J}^{(2)}$ is suggestive of a multiple crossing interpretation. If this is the case, the fact that the calculations cannot reproduce the $\mathcal{J}^{(2)}$ is not surprising, since this requires the calculations to reproduce the frequencies of the crossings and their interaction strengths very precisely.

In summary, four new SD bands have been observed in ^{86}Zr. Configuration-dependent shell correction calculations closely describe the properties of three of the bands. For example, crossings observed in two of the bands are well reproduced by the calculations. Interestingly, the calculations suggest that these bands correspond to triaxial SD shapes. In addition, the calculations are in agreement with the dynamic moment of inertia of SD1, which has a gradual downsloping trend with increasing rotational frequency. This is interpreted as a loss of collectivity as the quadrupole deformation of the band decreases, and the triaxiality of the nuclear shape increases. One of the four bands was found to have an unusually high moment of inertia. The calculations do not provide a satisfactory explanation for this band. It is suggested that the high moment of inertia of this structure results from multiple single particle crossings over the frequency range in which the band is observed.

Work supported in part by the U.S. DOE under Grant Nos. DE-FG05-88ER40406, DE-AC03-76SF00098, and in part by the Swedish Natural Science Research Council. ORNL is managed by Lockheed Martin Energy Research Corporation for U.S. DOE under Contract No. DE-AC05-96OR22464. A.V.A. and I.R. are grateful for financial support from the Royal Swedish Academy of Sciences.

[1] C. Baktash, in *Proceedings of the Conference on Nuclear Structure at the Limits*, Argonne National Laboratory, Argonne, Illinois, 1996 (ANL, Argonne, Illinois, 1997), p. 90.
[2] C. Svensson *et al.*, Phys. Rev. Lett. **79**, 1223 (1997).
[3] Gammasphere Proposal, Report LBNL-PUB-5202; I.Y. Lee, Nucl. Phys. **A520**, 361 (1990).
[4] D.G. Sarantites *et al.*, Nucl. Instrum. Methods Phys. Res. A **381**, 418 (1996).
[5] D.R. LaFosse *et al.* Phys. Rev. Lett. **78**, 614 (1997).
[6] D. Rudolph *et al.*, Phys. Lett. B **389**, 463 (1996).
[7] F. Cristancho *et al.*, Phys. Lett. B **357**, 281 (1995).
[8] M. Devlin *et al.*, Phys. Lett. B (in press).
[9] T. Bengtsson and I. Ragnarsson, Nucl. Phys. **A436**, 14 (1985).
[10] A.V. Afanasjev and I. Ragnarsson, Nucl. Phys. **A586**, 377 (1995).
[11] W. Nazarewicz *et al.*, Nucl. Phys. **A435**, 397 (1985).
[12] H. Schnack-Petersen *et al.*, Nucl. Phys. **A594**, 175 (1995).
[13] M. Devlin *et al.*, Nucl. Instrum. Methods Phys. Res. A **383**, 506 (1996).
[14] D.C. Radford, Nucl. Instrum. Methods Phys. Res. A **361**, 297 (1995).
[15] K.S. Krane *et al.*, Nucl. Data, Sect. A **11**, 351 (1973).
[16] B. Cederwall *et al.*, Nucl. Instrum. Methods Phys. Res. A **354**, 591 (1995).
[17] H.-Q. Jin *et al.*, Phys. Rev. Lett. **75**, 1471 (1995).
[18] A.V. Afanasjev and I. Ragnarsson, Nucl. Phys. **A608**, 176 (1996).